Developmental Cell
Article

Transcriptional Control of a Plant Stem Cell Niche

Wolfgang Busch,[1,6] Andrej Miotk,[2,5] Federico D. Ariel,[4,5] Zhong Zhao,[2] Joachim Forner,[2] Gabor Daum,[2] Takuya Suzaki,[2] Christoph Schuster,[2] Sebastian J. Schultheiss,[1] Andrea Leibfried,[1,7] Silke Haubeiß,[1,8] Nati Ha,[2,3] Raquel L. Chan,[4] and Jan U. Lohmann[1,2,*]

[1]AG Lohmann, Max Planck Institute for Developmental Biology, D-72076 Tübingen, Germany
[2]Department of Stem Cell Biology, Heidelberg Institute of Zoology
[3]CellNetworks–Cluster of Excellence and BIOQUANT Center
University of Heidelberg, D-69120 Heidelberg, Germany
[4]Laboratorio de Biotecnologia Vegetal, Instituto de Agrobiotecnologia del Litoral, Universidad Nacional del Litoral, Santa Fe, Argentina
[5]These authors contributed equally to this work
[6]Present address: Department of Biology and IGSP Center for Systems Biology, Duke University, Durham, NC, USA
[7]Present address: EMBL, 69117 Heidelberg, Germany
[8]Present address: Institute for Clinical Pharmacology, University Stuttgart, D-70376 Stuttgart, Germany
*Correspondence: jlohmann@meristemania.org
DOI 10.1016/j.devcel.2010.03.012

SUMMARY

Despite the independent evolution of multicellularity in plants and animals, the basic organization of their stem cell niches is remarkably similar. Here, we report the genome-wide regulatory potential of WUSCHEL, the key transcription factor for stem cell maintenance in the shoot apical meristem of the reference plant *Arabidopsis thaliana*. WUSCHEL acts by directly binding to at least two distinct DNA motifs in more than 100 target promoters and preferentially affects the expression of genes with roles in hormone signaling, metabolism, and development. Striking examples are the direct transcriptional repression of *CLAVATA1*, which is part of a negative feedback regulation of *WUSCHEL*, and the immediate regulation of transcriptional repressors of the TOPLESS family, which are involved in auxin signaling. Our results shed light on the complex transcriptional programs required for the maintenance of a dynamic and essential stem cell niche.

INTRODUCTION

Plant stem cells are embedded in specialized tissues called meristems, which are located at the growing points of the organism. These tissues provide an instructive environment for long-term stem cell maintenance and thus are regarded as stem cell niches similar to those found in animals (Scheres, 2007). However, in contrast to animal systems, in which individual stem cell niches only supply a defined organ system during adult development, almost the entire above-ground tissue of a plant is derived from the shoot apical meristem (SAM) (Weigel and Jürgens, 2002). Several key regulators of stem cell control in the SAM have previously been identified via genetic approaches in *Arabidopsis thaliana*. *WUSCHEL* (*WUS*) and *CLAVATA3* (*CLV3*) have opposing roles and are connected through a regulatory loop involving the receptor-like kinase CLAVATA1 (CLV1) (Brand et al., 2000; Clark et al., 1995, 1997; Laux et al., 1996; Schoof et al., 2000). Whereas *WUS* encodes a homeodomain transcription factor expressed in the organizing center within deeper layers of the SAM (Mayer et al., 1998), CLV3 is a small glycopeptide secreted from the stem cells (Fletcher et al., 1999; Kondo et al., 2006; Ohyama et al., 2009). CLV3 acts as a negative signal for stem cell proliferation, and by binding to the CLV1 receptor (Ohyama et al., 2009) leads to a transcriptional repression of *WUS*. In contrast, WUS has an instructive role for stem cell identity and is required for noncell autonomous induction and maintenance of stem cell fate. Consequently, stem cells differentiate prematurely and the shoot apical meristem collapses in *wus* mutants (Laux et al., 1996), whereas in *clv* mutants, stem cells proliferate abnormally, resulting in enlarged meristems (Clark et al., 1995).

Despite the central role of *WUS* for the shoot stem cell system only two direct targets have previously been identified: the floral homeotic gene *AGAMOUS* (*AG*) (Lohmann et al., 2001), and the A-type *Arabidopsis Response Regulator 7* (*ARR7*) (Leibfried et al., 2005). *AG* is activated by WUS in early flowers (Lohmann et al., 2001), where it lays down the basic floral pattern and terminates stem cell maintenance (Bowman et al., 1989). In contrast, WUS represses *ARR7* expression by binding to its promoter, thus counteracting the inhibitory activity of *ARR7* on cytokinin signaling in the center of the SAM (Leibfried et al., 2005; To et al., 2004). Although these two genes execute important functions downstream of WUS, they account for only a subset of WUS activity, and neither fully explains the role of WUS in inducing stem cell fate or the CLV-dependent feedback loop.

RESULTS

Genome-Wide Identification of *WUS* Response Genes

Because the regulatory circuitry of the SAM is highly interconnected and thus very stable, progress in elucidating the mechanisms downstream of *WUS* function in this tissue has been slow. In sharp contrast to the overall robustness of the SAM, complete loss of *WUS* or *CLV3* leads to drastic phenotypic variations, such as the lack of meristematic cells and developing organs or massive overproliferation of these tissues, respectively. To elucidate the mechanisms leading to stem cell induction downstream of *WUS* despite those difficulties, we used tools of systems

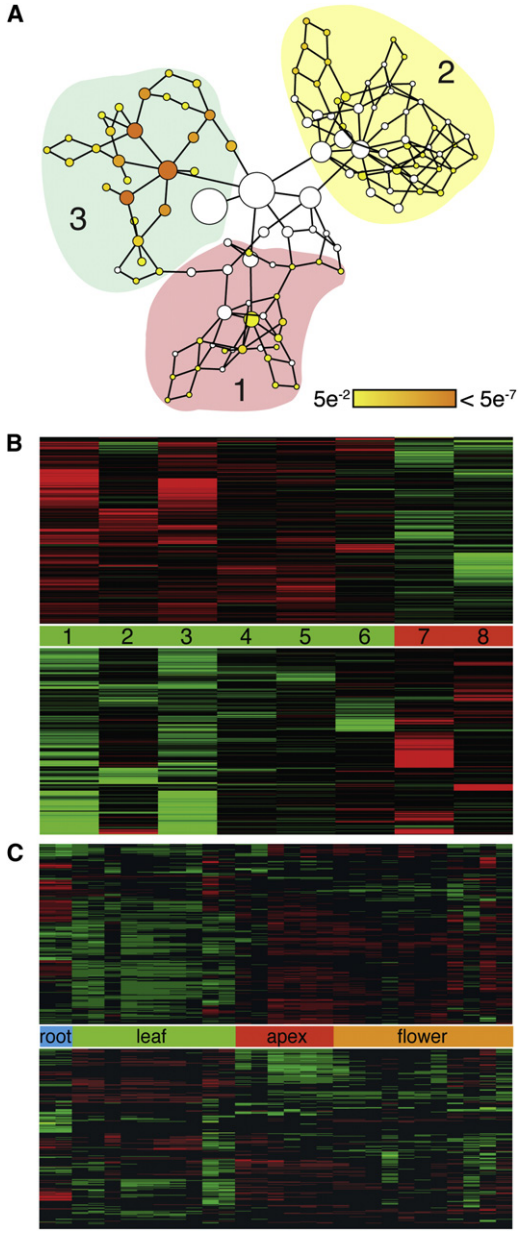

Figure 1. Function and Expression of *WUS* Response Genes

(A) Colored nodes represent statistically significantly enriched GO categories (FDR-corrected $p < 0.05$). The size of the nodes is proportional to the number of detected genes that belong to each category. The shaded areas encompass clusters that have been assigned to related GO categories: (1) regulation of development (meristem, cell death), (2) metabolism (tryptophane, glucosinolate), and (3) response to stimuli (defense, stress, hormones).

(B) Response of *WUS* downstream genes ($p < 0.01$) to modulation of *WUS* or *CLV3* activity. Samples that are labeled in green represent conditions with increased *WUS* activity; those in red denote decreased *WUS* levels. Samples: (1) *35S::AlcR,AlcA::WUS*, vegetative apex; (2) *35S::AlcR,AlcA::WUS II*, vegetative apex; (3) *35S::AlcR,AlcA::WUS*, inflorescence apex; (4) *35S::WUS:GR* (D), vegetative apex; (5) *35S::WUS:GR* (C+D), vegetative apex; (6) *clv3*, microdissected vegetative apex; (7) *35S::AlcR,AlcA::CLV3*, inflorescence apex; and (8) *wus*, microdissected vegetative apex. Upper panel: transcripts reduced by *WUS*. Lower panel: transcripts with increased abundance. Green indicates an increase in expression level, red indicates decreased expression; color intensity indicates the size of the effect.

biology to identify pathways directly linked to the WUS transcription factor. To this end, we recorded changes in the transcriptome after genetically perturbing the regulatory system of the stem cell niche at various developmental stages by loss-of-function and inducible overexpression alleles of *WUS* and its antagonist *CLV3* (Leibfried et al., 2005). The samples included microscopically dissected apices of *wus* and *clv3* mutants three days after germination, when the phenotypic consequences were still mild. However, because of the impeding phenotypes of these constitutive mutants, we used inducible overexpression alleles for most of the samples, which included apices of vegetative and flowering plants 4 and 12 hr after induction of *WUS* and *CLV3* overexpression, respectively. This allowed us to screen for the downstream effects of *WUS* independent of visible phenotypes during diverse developmental stages, because tissue was harvested before the induction of *WUS* or *CLV3* activity had caused morphological defects.

To identify target genes of the WUS transcription factor, the changes in the transcriptome resulting from the genetic perturbations were recorded by Affymetrix Ath1 microarrays in 15 independent experiments with at least two biological repetitions per sample. Because the transcriptional effects of WUS in each individual experiment were dictated by the specific regulatory environment represented by tissue context or developmental stage, we analyzed the entire dataset in a biologically coherent manner to capture most aspects of WUS function. To this end, we used a *Z*-score-based meta-analysis (Fulton et al., 2009) to identify WUS response genes, which allowed us to quantitatively correlate *WUS* activity with the expression levels of all genes across all datasets. First, we calculated the *Z*-score for all genes in every experiment-control comparison. We then integrated this information into the WUS regulations score (WRS) by adding up the *Z*-scores of each condition in which *WUS* activity was increased and subtracting *Z*-scores from each experiment with reduced *WUS* (see Experimental Procedures). Thus, the WRS quantitatively reflected the transcriptional behavior of every gene in response to modulation in *WUS* activity in relation to the average behavior of all genes.

For further analyses, we explored the statistical properties of the WRS. First, we tested whether the distribution of the WRS was skewed toward negative or positive values and found that it was centered around 0 with a mean of 4×10^{-8} without significant skew (see Figure S1A available online). Next, we empirically determined a significance threshold for the WRS by random sampling (WRS $\pm 7.99 = p < 0.01$). Applying this cutoff to our dataset, we identified 675 *WUS* response genes, which include transcripts that are dependent on WUS activity either directly or through mediator genes. It is important to note that the directionality of the WRS does not necessarily reflect the activity of WUS when acting on direct targets, because direct and indirect effects were analyzed at once by pooling static and dynamic

(C) Expression profiles of *WUS* response genes during *Arabidopsis* development as assayed by representative conditions of AtGenExpress (Schmid et al., 2005) (see Supplemental Experimental Procedures). Upper panel: transcripts reduced by *WUS*. Lower panel: transcripts with increased abundance. Green indicates higher expression than average; red indicates lower expression than average. For more information on the WRS and response genes, see Figure S1 and Table S1.

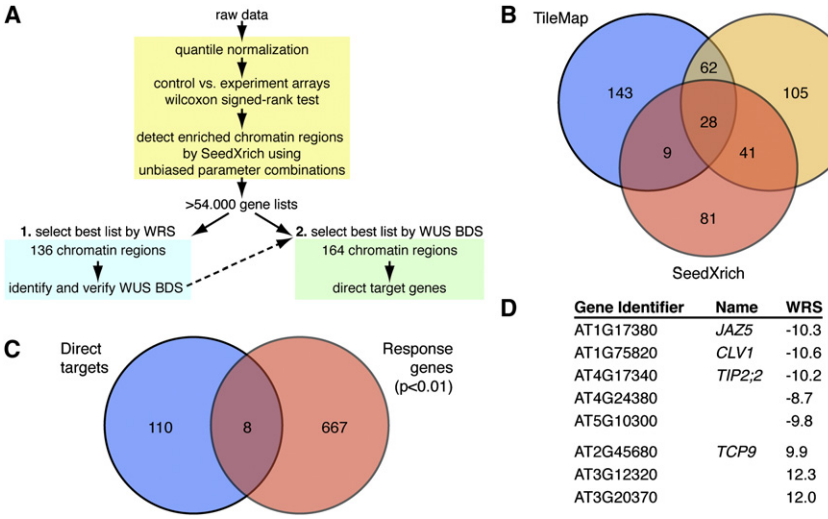

Figure 2. Analysis Pipeline and Results of WUS ChIP-chip

(A) Flowchart of ChIP-chip analysis pipeline.

(B) Comparison of ChIP-chip results obtained by alternative detection algorithms TileMap, MAT, and SeedXrich. Numbers denote genes that were assigned to the enriched chromatin regions identified by the algorithms.

(C) Overlap of WUS direct targets and WUS response genes.

(D) List of direct WUS targets with significant WRS. For statistical evaluation of detection algorithms, see Figure S2. Detected chromatin regions are listed in Table S2.

experiments. However, because the WRS was based on a unified analysis of our diverse set of experiments, it should capture WUS activity much more robustly than analyses of individual experiments. We observed a good correlation between expression changes of response genes and WUS activity across most samples (Figure S1B). In contrast, we did not observe such significant correlations when analyzing all genes, because the individual samples differed substantially and microarray experiments are inherently noisy (Figure S1C). Thus, through our use of the meta-analysis-based WRS, we were able to efficiently detect WUS response genes, which followed a consistent expression trend across a diverse set of regulatory environments.

Consequently, the 675 transcripts identified included four *ARR* genes previously described as WUS targets (Leibfried et al., 2005) (Figure 1; Table S1). In addition, the response genes included *PERIANTHIA* (*PAN*), which encodes a bZIP transcription factor expressed in the SAM and floral meristems. *PAN* and *WUS* expression not only overlap in these tissues, but in addition *PAN* has recently been shown to be stimulated by *WUS* activity (Maier et al., 2009). In contrast, the floral homeotic gene *AGAMOUS* (*AG*) was not found among the response genes, even though it had been shown to be a direct target gene of WUS (Lohmann et al., 2001). This is consistent with the restriction of the *WUS-AG* regulatory interaction to flowers and our sampling, which had been focused on vegetative stages. Taken together, these findings demonstrate the validity and sensitivity of our meta-analysis strategy, prompting us to quantitatively investigate WUS response genes.

Global Analysis of *WUS* Response Genes

We first asked where and when *WUS* response genes were active by analyzing their expression profiles in the AtGenExpress dataset (Schmid et al., 2005). We found that transcripts whose expression was reduced by *WUS* were mainly expressed in leaves, whereas transcripts with increased abundance were more likely to be active in the apex and flowers (Figure 1C). This is consistent with the expression of *WUS*, which is limited to the apex, as well as the biological function of *WUS*, because genes with high expression in leaves are more likely to be associated with transcriptional programs of differentiated cells, a function supposedly repressed by *WUS*. Following the analysis of tissue-specific expression of WUS response genes, we interrogated their expression within the SAM. To this end, we used the transcriptome dataset by Yadav et al. (2009), which was generated from sorted cells of the *apetala1/cauliflower* double mutant. This mutant combination produces floral meristems that are partially converted into inflorescence meristems and thus provides a resource for a large number of SAM-like cells (Bowman et al., 1993). For this dataset, transcriptome profiles were obtained from sorted cells that were labeled by fluorescent proteins expressed from the *CLV3*, *WUS*, or *FILAMENTOUS FLOWER* (*FIL*) promoter, respectively (Yadav et al., 2009). When we compared this dataset with our *WUS* response genes, we found that genes with significant WRS were overrepresented among the transcripts with expression specific to subdomains of the SAM. Interestingly, genes whose expression was reduced by *WUS* were most strongly enriched among RNAs found only in the *WUS* domain. In contrast, *WUS* response genes that were activated were strongly enriched among the transcripts expressed specifically in the combined *CLV3* and *WUS* and the combined *CLV3* and *FIL* domains, respectively (Figure S1D). These results are in line with our expectations and suggest that our list of *WUS* response genes contains direct as well as indirect target genes, which differ in their SAM expression. The bias toward transcripts with reduced expression in the *WUS* domain suggests that WUS primarily acts as a transcriptional repressor (Ikeda et al., 2009; Leibfried et al., 2005) with roles in modulating target gene expression rather than providing binary on/off inputs.

Having shown that WUS response genes have nonrandom expression patterns, we next explored the biological functions associated with the pathways controlled by *WUS*. Although the number of *WUS* response genes was large, many of them had functions in three groups of related biological processes as identified by gene ontology (GO) (Figure 1A; Table S1): (1) regulation of development, including meristem and stem cell maintenance as well as apoptosis; (2) metabolic processes, among them biosynthesis of auxin precursors; and (3) response to various stimuli, such as auxin and cytokinin signaling. Interestingly, several genes with positive roles in auxin signaling (such as

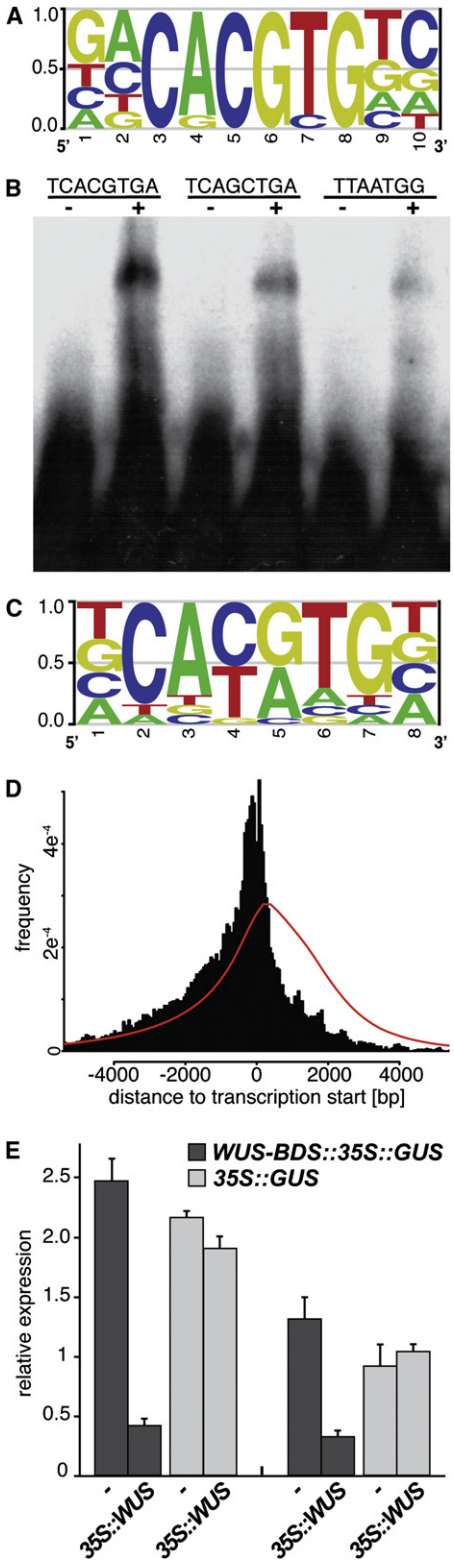

Figure 3. Chromatin and DNA Binding Preferences of WUS

(A) Position frequency matrix derived from ChIP-chip data as identified by MDscan.

(B) EMSA using recombinant WUS protein purified from *E. coli* with probe sequences derived from ChIP-chip sampling and the *AG* intron (TTAATGG).

(C) Position weight matrix derived from EMSA.

(D) Distances of WUS binding regions from the nearest annotated transcription start. The red line indicates background distribution.

(E) Reporter gene assay demonstrating the functional relevance of the TCACGTGA element for mediating transcriptional responses to WUS. Quantitative real-time RT-PCR on *N. benthamiana* leaves with reporter genes either including the G-Box WUS binding site (*WUS-BDS::35S::GUS*) or without WUS binding site (*35S::GUS*) coinfiltrated with or without a *WUS* expressing construct (*35S::WUS*). Two independent experiments were performed, each of which was assayed in triplicate. Error bars indicate the standard error of the mean. For information on WUS homo-dimerization see Figure S3. The results of the SELEX sequence decompositions are listed in Table S3.

biosynthesis or response), as well as many with negative roles in cytokinin signaling (such as cytokinin breakdown or negative feedback regulation), were among the transcripts with reduced expression. The abundance and diversity of response genes suggests that *WUS*-dependent meristem maintenance is likely governed by a complex regulatory machinery rather than by a small number of executive genes.

Genome-Wide Identification of Chromatin Regions Bound by WUS In Vivo

As a first step to elucidate the topology of the *WUS*-dependent network, we identified regions of the genome directly bound by WUS using chromatin immunoprecipitation (ChIP). We used a polyclonal antiserum against WUS (Leibfried et al., 2005) (Figure S2A) and genome-wide detection on Affymetrix whole-genome tiling arrays, which provide a 35-bp resolution across the nonrepetitive regions of the *A. thaliana* genome. In total, we performed 13 independent ChIP-chip hybridizations using apices of seedlings carrying an inducible *WUS* allele, as well as *wus* mutant seedlings as controls. We analyzed the resulting hybridization patterns in a two-step procedure (Figure 2A) using published detection algorithms, TileMap and MAT (Ji and Wong, 2005; Johnson et al., 2006), as well as a seed extension algorithm that we developed (SeedXrich; see Experimental Procedures). First, we computed a statistical measure of difference between experimental and *wus* mutant control hybridizations by a nonparametric sliding window analysis. This step eliminated effects by unspecific interaction of the antibody with WUS-related proteins as well as sequence-dependent hybridization artifacts from the tiling array. As a second step, we scanned the entire genome for significantly enriched regions using SeedXrich, MAT, or TileMap, respectively (Figure 2B). The hybridization patterns of ChIP-chip experiments are notoriously variable and therefore most detection algorithms can be adjusted to the nature of the raw data by several parameters in order to successfully identify enriched chromatin regions. The variables typically include the level of confidence in enrichment at individual array probe locations, the number of adjacent probes above a certain threshold, as well as the number and size of gaps allowed in a significantly enriched region. These parameters closely define what types of hybridization signals are picked up as positives and thus have a major impact on the resulting target region prediction. Therefore, we systematically explored this parameter space by calling enriched regions using a wide variety of unbiased parameter combinations resulting in more than 54.000 gene lists (Figure 2A). Working under the assumption that response genes should be overrepresented

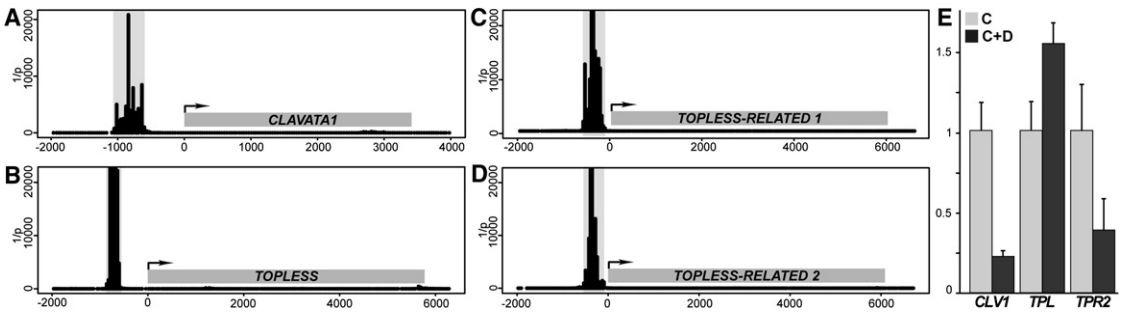

Figure 4. WUS Binding to Upstream Regions of *CLV1* and *TPL*/*TPR* Genes and Resulting Regulatory Effects

(A–D) WUS binding signatures as shown by inverted p values (*y* axis) from the experiment-control comparison. Genomic positions (*x* axis) are given relative to the annotated transcription start of the indicated primary RNA. Shaded areas indicate genomic regions that were detected as enriched.

(E) Expression of *CLV1*, *TPL*, and *TPR2* 4 hr after induction of WUS activity in the presence of the protein biosynthesis inhibitor cycloheximide. Light gray bars represent cycloheximide-only controls (C), dark gray bars indicate cycloheximide and dexamethasone induction (C+D). Expression levels are linearly transformed gcRMA expression estimates from duplicate Affymetrix Ath1 hybridizations. Cycloheximide controls have been normalized to 1. Error bars indicate the standard error of the mean. See Table S4 for the list of direct target genes and Figure S4 for analyses of their response to altered WUS activity.

among the direct WUS targets, we then used permutation testing to identify the list that contained the highest overrepresentation of genes with significant WRS. SeedXrich outperformed TileMap and MAT in picking up parts of the genome that are linked to genes with significant WRS, and the parameter optimization converged on very stringent detection settings (probe p value seed, $p < 0.0004$; probe p value, $p < 0.002$; minimum length of hybridization, 10 probes; maximum gap, three probes). This suggested that inclusion of a larger number of binding events would lead to the increased identification of false-positives (Figures S2B and S2C).

This biologically motivated parameter exploration using expression information as a benchmark resulted in the identification of 136 chromatin regions bound by WUS in vivo (Table S2). When we compared the results obtained by our SeedXrich algorithm with the established MAT and TileMap programs, we found an overlap similar to the one observed between TileMap and MAT (Figure 2B).

DNA and Chromatin Binding Preferences of WUS

Having reliable in vivo target regions of WUS allowed us to sample the sequences of those fragments for potential *cis*-regulatory elements, which could mediate the activity of WUS. In addition to the known WUS-binding motif (Lohmann et al., 2001), we found a highly overrepresented motif (Figure 3A) using two independent algorithms (Ettwiller et al., 2007; Liu et al., 2002). Because this motif was a G-Box (Menkens et al., 1995) and unrelated in sequence to the only known WUS binding sequence from the *AG* enhancer (Lohmann et al., 2001), we used electrophoretic mobility shift assays (EMSAs) using recombinant WUS from *Escherichia coli* and yeast to validate both binding sequences (Figure 3B). Because WUS interacted with both the G-box and the known TAAT motif from the *AG* enhancer despite their divergent sequences (Figure 3B), we asked whether additional binding sites might exist. Therefore, we performed systematic evolution of ligands by exponential enrichment (SELEX) using the WUS homeodomain to identify all potential binding sequences. After seven rounds of SELEX, two classes of sequences were enriched (Table S3). The first class contained TCA sequences, whereas the second class contained AAT cores, supporting our ChIP-chip results and the previously published binding site, respectively (Lohmann et al., 2001). However, the SELEX motifs were much shorter and not palindromic, likely because of differences in WUS conformation. Whereas SELEX was performed using only the N-terminal homeodomain for reasons of protein stability, we found that WUS homodimerizes via structures in the C terminus (Figure S3) similar to its ortholog from rice (Nagasaki et al., 2005). Thus, SELEX identified monomer binding sequences, whereas ChIP-chip-derived motifs were likely bound by homodimers.

To compare the relative affinities of the previously published and the G-Box binding sequence, we measured the dissociation constant (K_D) of full-length WUS for both motifs. The TCACGTGA sequence was bound with 20-fold higher affinity than a TAAT-containing element from the *AG* enhancer with K_D = 1.6-7 M and 3.0-6 M, respectively. Using this information, we established a consensus in vitro binding motif for WUS via systematic variation of nucleotides starting from the G-box motif (Figure 3C). The in vivo and in vitro motifs largely overlapped in sequence; however WUS seemed to exhibit stricter binding specificity when binding to chromatin in vivo (Figures 3A and 3C).

After having established that WUS binds to the TCACGTGA motif in vivo and in vitro, we explored the function of this DNA element by reporter gene analysis in plant cells. To this end, we fused a multimer containing five copies of the G-Box motif to the 5′ end of the constitutive 35S promoter derived from the cauliflower mosaic virus and a *GUS* reporter gene immediately downstream of this synthetic promoter (*WUS-BDS::35S::GUS*). This reporter construct was infiltrated into *Nicotiana benthamiana* leaves either alone or together with a *WUS* overexpression plasmid (*35S::WUS*). Leaves transformed with a reporter construct without the *WUS* binding site (*35S::GUS*) with and without *WUS* overexpression served as controls. Four days after infiltration, leaves were harvested and *GUS* expression was analyzed using quantitative real-time RT-PCR. We observed a strong reduction in reporter gene activity in response to *WUS* when the WUS binding site was present, whereas the reporter without the TCACGTGA element did not respond to equivalent levels of *WUS* overexpression (Figure 3E). These results demonstrated that WUS is able to act as a potent transcriptional

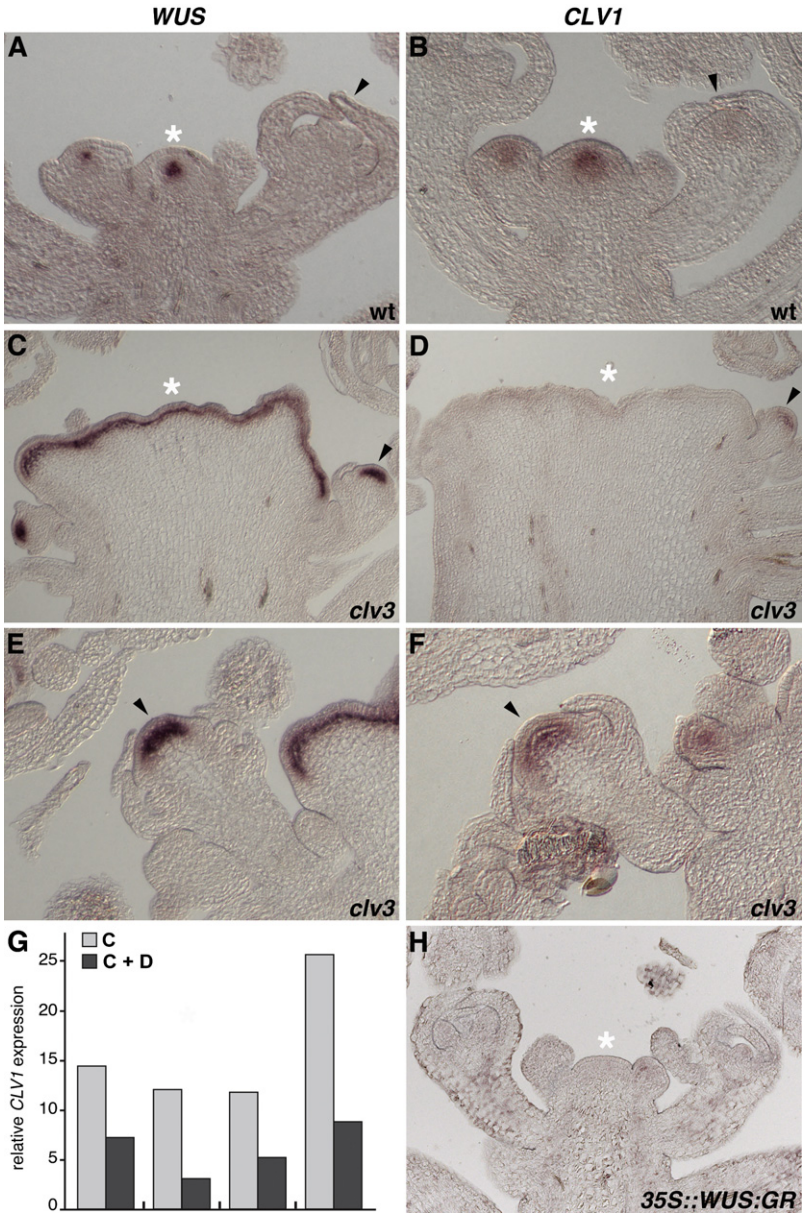

Figure 5. Expression Patterns of *WUS* and *CLV1* in Apices of Wild-Type and *clv3* Mutants

WUS and *CLV1* RNA in situ hybridizations on tissue sections of inflorescence apices.

(A, C, and E) *WUS* probe.

(B, D, F, and H) *CLV1* probe.

(A and B) Wild-type, (C–F) *clv3* mutant, and (H) *35S::WUS-GR* after 4 hr of induction with dexamethasone. Asterisks denote shoot apical meristems; arrowheads mark floral meristems.

(G) Expression of *CLV1* in apices of *35S::WUS-GR* seedlings following 4 hr of cycloheximide treatment (C) or cycloheximide with dexamethasone induction (C+D) as measured by quantitative real-time RT-PCR. Four independent experiments were performed, each of which was assayed in duplicate. For more information on the expression of *CLV1* and the interaction of *CLV1* and *CLV3* with *WUS*, see Figure S5.

repressor and that the G-Box binding motif efficiently mediates regulatory inputs by WUS even when taken out of context.

Refined Identification of In Vivo WUS Target Regions

Knowledge of a validated WUS binding site allowed us to reanalyze our ChIP experiments using the occurrence of the G-Box in target regions as benchmark. We reasoned that such a sequence-based parameter optimization would increase the detection accuracy because our initial selection exclusively relied on expression information and thus was dependent on the assignment of genes to chromatin regions. Furthermore, the Ath1 expression array includes only 75% of the annotated *A. thaliana* genes. In contrast, the occurrence of TCACGTGA elements as benchmark for selecting the relevant list of chromatin fragments should allow an unbiased whole genome scan for WUS binding regions. Thus, we reanalyzed the large number of SeedXrich output lists to identify the set of chromatin regions that showed the highest overrepresentation of WUS binding sites via permutation analysis (Figure 2A). The highest scoring list contained 164 target regions (Table S2), and the detection settings associated with this list were again very stringent (probe p value seed, $p < 0.00006$; probe p value, $p < 0.002$; minimum length of hybridization, six probes; maximum gap, one probe). By mapping those fragments to the *A. thaliana* genome, we found that WUS has a strong preference for binding within 500 bp upstream of transcription start sites (Figure 3D). This fits well with the underrepresentation of polymorphisms and the large number of predicted *cis*-regulatory elements in this region (Zeller et al., 2008) and demonstrated that WUS primarily acts in close proximity to the basal transcription machinery. In addition to the G-Box element, we also found an overrepresentation of TAAT elements in the WUS-bound regions. Most notably, the previously characterized TTAATGG motif was 4-fold enriched over background sequences.

Nature and Function of Direct WUS Targets

To analyze how WUS activity is translated into cell behavior, we called direct WUS target genes that were in proximity of the 164 identified chromatin regions (Figure 2A). However, not every region could be assigned to a single gene, whereas others were in regions of the genome that did not have annotated genes. The resultant list of direct WUS targets contained 159 annotated genes, 118 of which were represented on the Ath1 expression array (Table S4). Despite the fact that expression information was not used to identify the direct targets, WUS response genes were overrepresented and accounted for 7% of the direct targets (8 out of 118 at $p < 0.01$ WRS) (Figures 2C

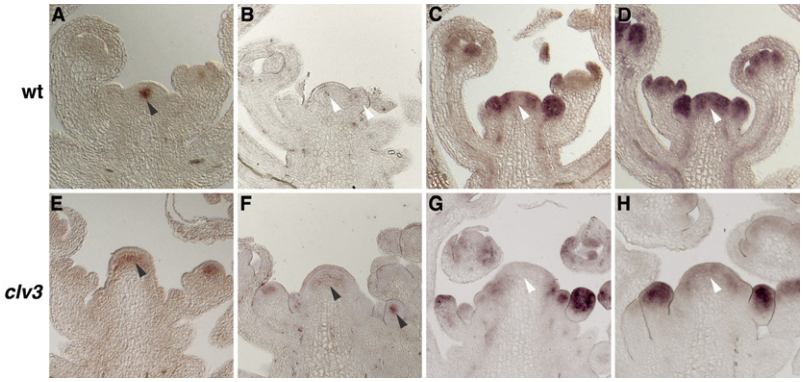

Figure 6. Expression Patterns of *WUS*, *TPL*, *TPR1*, and *TPR2* in Wild-Type and *clv3* Mutant Inflorescence Apices

WUS, *TPL*, *TPR1*, and *TPR2* RNA in situ hybridizations on tissue sections of inflorescence apices.
(A and E) *WUS* probe.
(B and F) *TPL* probe.
(C and G) *TPR1* probe.
(D and H) *TPR2* probe.
(A–D) Wild-type inflorescence apices.
(E–H) *clv3* mutant inflorescence apices. Gray arrowheads indicate expression; white arrowheads denote absence or low levels of *TPL*, *TPR1*, and *TPR2*.

and 2D). These numbers are in line with published results for other transcription factors, which reported that on average only 1%–10% of direct targets show transcriptional responses to the bound transcription factor (Farnham, 2009). However, these studies typically investigate a larger number of direct targets and rely on smaller expression data sets in more complex genomic backgrounds. The low convergence of direct WUS targets and response genes either suggests that most of the WUS binding sites are nonfunctional or that only a small number of cells is able to properly respond to WUS activity. Alternatively, our ChIP-chip experiment could overestimate binding, which seems unlikely given the small number of WUS binding events recorded in our study. Despite the low overlap with direct targets, our meta-analysis-based WRS was more powerful in identifying response genes than analyses of individual samples (e.g., the *35S::WUS-GR* C+D experiments) (Figure S4). In addition, the expression patterns of direct WUS targets were biased toward activity in the center of the meristem, because they were more than 2-fold overrepresented among genes with specific expression in the *WUS* domain, whereas such enrichment could not be detected for the *CLV3* and *FIL* domains (Figure S1D).

A striking example of a yet unknown direct target was *CLV1*, which had a strong WUS binding signature including a canonical TCACGTGA binding motif 600 bp upstream of the transcription start site (Figure 4A). In addition, *CLV1* mRNA expression was significantly reduced in response to ectopic *WUS* activity even in the absence of protein synthesis (Figure 4E). *CLV1* has important roles in SAM function and encodes a leucine-rich repeat receptor-like kinase, which is involved in the transcriptional repression of *WUS* by CLV3 (Clark et al., 1997; Ohyama et al., 2009). The capacity of WUS expression to self organize (Reinhardt et al., 2003) implied an autoregulatory mechanism for *WUS*, and our results suggest that *WUS* might sustain its own expression by directly repressing the transcription of one of its most important repressors. To study this interaction on a cellular level, we analyzed *WUS* and *CLV1* expression in wild-type and *clv3* mutants (Trotochaud et al., 1999) (Figure 5). Shoot meristems of *clv3* plants are greatly enlarged due to expanded *WUS* expression. Thus, if *CLV1* expression was independent of *WUS*, the *CLV1* RNA domain should be expanded; however, if WUS was a repressor of *CLV1* transcription, ectopic WUS activity should counteract this effect. Consistent with the latter scenario, *CLV1* RNA was hardly detectable in the central region of *clv3* mutant SAMs, whereas we picked up hybridization signal from the SAM periphery and developing flowers (Figure 5D).

To further validate a direct regulatory interaction between WUS and *CLV1*, we made use of *35S::WUS-GR* lines, in which WUS activity can be ectopically induced in the absence of protein synthesis (Brand et al., 2002; Leibfried et al., 2005; Lenhard et al., 2002). Using quantitative real-time RT-PCR on four independent biological experiments, we confirmed that the reduction of *CLV1* expression by WUS is independent of protein synthesis and thus likely direct (Figure 5G). In addition, in situ hybridization on inflorescences of dexamethasone-treated *35S::WUS-GR* plants demonstrated that expression of *CLV1* in the SAM was virtually abolished (Figure 5H), consistent with our results from in vivo and in vitro binding and reporter gene studies. Interestingly, *WUS* and *CLV1* RNA expression domains overlapped in wild-type apices (Clark et al., 1997) (Figure 5A and 5B; Figure S5A), suggesting that WUS does not act as a binary switch for *CLV1* expression, but rather is involved in fine-tuning its expression levels. To elucidate the consequences of this interaction for the regulatory machinery of the SAM, we simulated the *WUS*/*CLV3* feedback using a simple modeling tool (Vercruysse and Kuiper, 2005) and found that the repression of *CLV1* by *WUS* promoted the adaptation of the *WUS*/*CLV3* feedback to equilibrium over a wide range of experimental parameters (Figure S5B).

Another striking finding was that WUS acts directly upstream of three out of five members of the *TOPLESS*/*TOPLESS-RELATED* (*TPL*/*TPR*) family of transcriptional corepressors (Figures 4B–4D), which have essential roles in embryonic patterning and auxin response (Long et al., 2006; Szemenyei et al., 2008). We found strong WUS binding signatures in the promoters of *TPL*, *TPR1*, and *TPR2* and a transcriptional response to *WUS* activity even when protein synthesis was inhibited by cycloheximide, suggesting a direct regulatory interaction. Whereas expression of *TPL* was increased following induction of *WUS*, the abundance *TPR2* RNA was reduced (Figure 4E). *TPR1* was not represented on the expression array.

We then investigated with cellular resolution whether the expression patterns of *TPL*, *TPR1*, and *TPR2* are compatible with the regulatory interactions observed on the systems level. Consistent with a negative role of WUS, we found strong expression of *TPR1* and *TPR2* in the periphery of the SAM, which was excluded from the *WUS* expression domain (Figures 6C and 6D). At the same time, we observed strong *TPR1* and *TPR2*

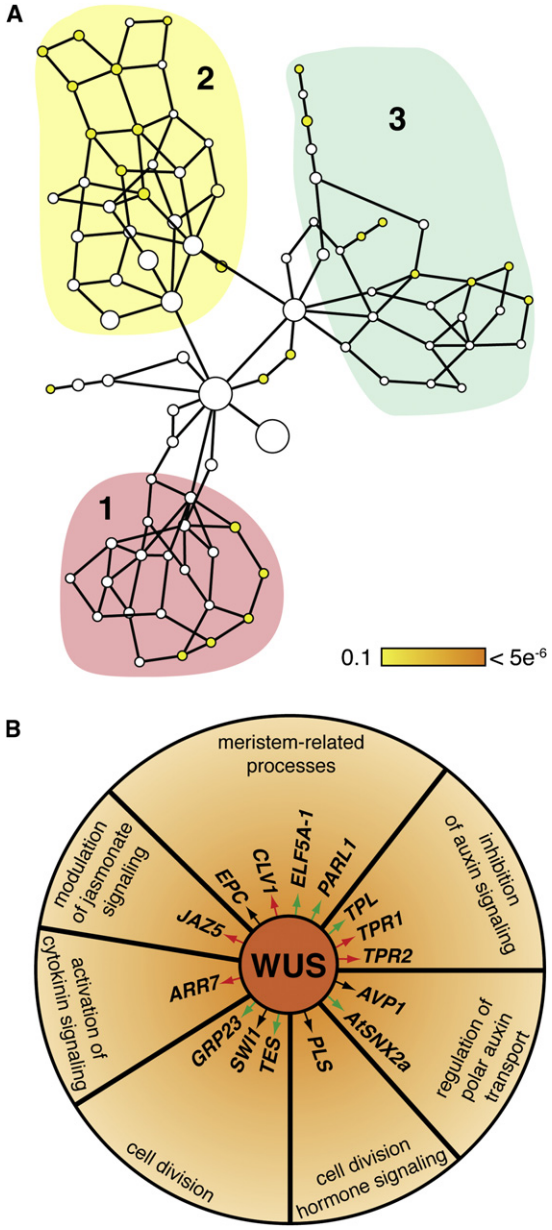

Figure 7. Function of Direct *WUS* Targets

(A) Colored nodes are significantly enriched GO categories (FDR-corrected $p < 0.1$). The size of the nodes is proportional to the number of detected genes that belong to each category. The shaded areas encompass clusters that have been assigned to related GO categories: (1) tissue development, meristem, and pattern specification processes; (2) monosaccharid metabolism; and (3) cell division processes. See Table S5 for information on enriched GO categories and respective p values.

(B) Biological function of developmentally relevant direct WUS target genes (Table 1). Green arrows indicate induction by WUS (positive WRS or data from qRT-PCR or in situ hybridization), red arrows indicate repression by WUS (negative WRS or data from qRT-PCR or in situ hybridization), and black arrows denote neutral interactions or lack of expression data.

expression in young flowers in domains overlapping with *WUS* RNA, suggesting that in the context of flower development, these genes might be activated by WUS rather than repressed. Consistent with such a complex regulatory interaction (Ikeda et al., 2009), *TPR1* and *TPR2* transcripts were absent from the *WUS* expression domain in expanded SAMs of *clv3* mutants, whereas they accumulated to high levels in the adjacent flower primordia (Figures 6G and 6H). Although we were unable to detect *TPL* expression in the wild-type SAM as reported by Kieffer et al. (2006), we observed *TPL* RNA accumulation in *WUS* expressing cells of *clv3* apices (Figures 6B and 6F), confirming the activation of *TPL* by WUS identified at the systems level (Figure 4E).

In addition to a transcriptional regulation by WUS, TPL was shown to interact with WUS protein and expression of *WUS* alleles, which lack the TPL interaction domain to cause dominant negative phenotypes (Kieffer et al., 2006). This complex multitier interaction with the *TPL/TPR* genes and proteins tightly links *WUS* to the local modulation of auxin signaling. In line with the essential function of the WUS-TPL machinery, the deduced regulatory wiring consisted of a coherent feed-forward loop with AND logic, which results in robustness against activation by random fluctuations (Alon, 2007).

To elucidate the functions executed by direct WUS targets quantitatively, we subjected them to GO category analysis (Figure 7A; Table S5). We found that genes with roles in development and differentiation were overrepresented with many involved in cell division and hormone signaling. Literature mining revealed that corresponding mutants frequently cause developmental defects (Figure 7B, Table 1), which are not limited to the SAM, suggesting that they have pleiotropic functions downstream of WUS in other tissues, or that they act redundantly in the SAM. These findings were consistent with the known roles of WUS in reproductive tissues (Deyhle et al., 2007; Gross-Hardt et al., 2002; Lohmann et al., 2001), as well as the observation that SAM function is redundantly regulated.

DISCUSSION

Taken together, our results demonstrate that WUS affects the expression of a large set of downstream genes, including many transcripts with roles in development and signaling. Although it is known that WUS affects cytokinin signaling (Leibfried et al., 2005), we show here that WUS has the potential to negatively influence auxin biosynthesis and perception, suggesting that regulation of the cytokinin/auxin balance is central to SAM function. In addition, we show that WUS negatively modulates the *CLV* pathway via repression of *CLV1*, adding another layer of complexity to the regulatory circuit of the SAM. Thus, our results demonstrate at the systems level that one of the primary roles of WUS in setting up the stem cell niche in the SAM is to locally orchestrate cellular responses to mobile signals. It seems likely that these effects are not mediated by a few master executive regulators, but by more than 100 direct transcriptional targets. Similar numbers have also been reported for homeodomain transcription factors of the Hox class (Hueber et al., 2007).

To orchestrate the expression of direct target genes, WUS binds to at least two divergent DNA sequence motifs. The substantial difference in binding affinity suggests that WUS might regulate distinct sets of targets in a concentration-dependent manner. Recent studies have shown that DNA binding specificities of animal homeodomain transcription factors are

Table 1. Reference Table for Developmentally Relevant Direct WUS Target Genes

Gene-ID	WRS	Gene Name	Evidence	Reference
AT1G15750	0.9	WUS-INTERACTING PROTEIN 1 (WSIP1); TOPLESS (TPL)	Phenotype	(Long et al., 2006; Szemenyei et al., 2008)
AT1G80490	N.A.	TOPLESS-RELATED 1 (TPR1)	Inference	(Long et al., 2006; Szemenyei et al., 2008)
AT3G16830	2.8	TOPLESS-RELATED 2 (TPR2)	Inference	(Long et al., 2006; Szemenyei et al., 2008)
AT1G15690	0.9	*ARABIDOPSIS THALIANA* V-PPASE 3 (ATAVP3); (AVP-3); (AVP1)	Phenotype	(Li et al., 2005)
AT5G58440	1.8	SORTING NEXIN 2a (SNX2a)	Inference	(Jaillais et al., 2006)
AT4G39403	N.A.	POLARIS (PLS)	Phenotype	(Chilley et al., 2006)
AT3G43210	2.1	TETRASPORE (TES)	Phenotype	(Tanaka et al., 2004)
AT5G51330	N.A.	SWITCH1 (SWI1); (DYAD)	Phenotype	(Agashe et al., 2002; Siddiqi et al., 2000)
AT1G10270	7.8	GLUTAMINE-RICH PROTEIN23 (GRP23)	Phenotype	(Ding et al., 2006)
AT1G17380	−10.3	JASMONATE-ZIM-DOMAIN PROTEIN 5 (JAZ5); (tify11a)	Inference	(Chini et al., 2007; Thines et al., 2007)
AT3G55830	0.2	ECTOPICALLY PARTING CELLS (EPC1)	Phenotype	(Singh et al., 2005)
AT1G75820	−10.6	CLAVATA 1 (CLV1)	Phenotype	(Brand et al., 2000; Clark et al., 1993; Clark et al., 1997; Ogawa et al., 2008; Schoof et al., 2000)
AT1G13950	6.7	EUKARYOTIC ELONGATION FACTOR 5A-1 (ELF5A-1)	Inference	(Feng et al., 2007)
AT1G48920	3.4	PARALLEL 1 (PARL1); (ATNUC-L1)	Phenotype	(Kojima et al., 2007; Petricka and Nelson, 2007)

more diverse than previously anticipated (Berger et al., 2008; Noyes et al., 2008). We found WUS to be most similar to zinc-finger homeodomain factors and strikingly, Zfh-1, the closest relative from *Drosophila*, has important roles in the self-renewal of testis stem cells (Leatherman and Dinardo, 2008). In addition, Zeb-1, the human ortholog of Zfh-1, has been shown to bind to CANNTG sequences (Grooteclaes and Frisch, 2000), which are contained within the G-Box WUS DNA binding motif. The sequence of this binding site is also identical to the one bound by the bHLH-ZIP transcription factor MYC (Blackwell et al., 1990), an essential growth regulator conserved throughout animal evolution (Eilers and Eisenman, 2008), which is required for induction of pluripotent stem cells (Takahashi and Yamanaka, 2006). Thus, our work suggests that the mechanism of stem cell control in plants and animals might be less diverse than previously thought.

EXPERIMENTAL PROCEDURES

Plant Material and Treatments

Plants were of Columbia (Col-0) background and grown on soil at 23°C in continuous light at 65% relative humidity. The *wus* allele used in this study corresponded to *wus-4* in Columbia (from Martin Hobe and Rüdiger Simon). *35S::AlcR;AlcA::WUS*, *35S::AlcR,AlcA::CLV3*, *35S::AlcR,AlcA::GUS*, and *35S::WUS-GR* lines were described by Leibfried et al. (2005). *35S::WUS-GR* plants were grown on 0.8% agar with half-strength Murashige and Skoog media at 23°C under 16 hr of light. Ethanol inductions were performed at 20°C by watering with 1% ethanol. For dexamethasone induction, tissue was harvested and incubated for 4 hr in 15 μM dexamethasone and 0.015% Silwet L-77. Cycloheximide was used at 10 μM.

Microarray Experiments

For the mutant analysis, shoot apices of 45 seedlings were microdissected 3 days after germination and RNA was extracted from pooled apices. Each experiment was conducted in triplicate and repeated twice. For the induction series, 25 microdissected apices of plants, which had been induced with 1% ethanol for 12 hr, were used. The *35S::AlcR;AlcA::WUS* data were published previously (Leibfried et al., 2005). For the *35S::WUS-GR* series, 15 plants per sample were grown on plates for 10 days before harvest and induction for 4 hr. Each experiment was conducted in duplicate. Samples were prepared and hybridized to Affymetrix Ath1 arrays as described by Leibfried et al. (2005). Expression estimates were calculated using gcRMA implemented in R with standard settings (Gentleman et al., 2004; Wu et al., 2004). A TAIR7-based Cdf/Probe/Annotation Package was used from http://brainarray.mbni.med.umich.edu/Brainarray/Database/CustomCDF/CDF_download_v10.asp for probe mapping. Expression estimates were transformed to a linear scale and averaged and fold change (FC) was calculated for every gene. A *Z*-score for each fold change was calculated by dividing the difference of $\log_2$-transformed FC and the mean of the FC population by the standard deviation of the FC population:

$$\left(Z = \frac{\log_2(FC) - \overline{\log_2(FC)}}{\sigma_{\log_2 FC}}\right).$$

To create the WRS for every gene, the sum of the *Z*-scores of the conditions with reduced *WUS* was subtracted from the sum of the *Z*-scores of the conditions in which *WUS* was overactivated:

$$\mathrm{WRS} = \left(Z_{\mathrm{AlcA::WUS1}} + Z_{\mathrm{AlcA::WUS2}} + Z_{\mathrm{AlcA::WUSfl}} + Z_{\mathrm{WUS-GR\_D}} + Z_{\mathrm{WUS\text{-}GR\_CD}} + Z_{clv3}\right) - \left(Z_{\mathrm{AlcA::CLV3-1}} + Z_{wus}\right)$$

An empirical p value for the WRS was calculated by 10,000-fold random sampling of individual WRS values.

Western Blotting

Nuclear protein was extracted in 50 μl SDS-Sample buffer (310 mM Tris pH 6.8, 50% glycerol, 10% SDS, 0.5% bromphenol blue, 3.5% mercaptoethanol) for 10 min at 95°C and used for standard SDS-PAGE and western blotting. Signals were captured using an INTAS chemiluminescence detection station.

ChIP Assay

ChIP was conducted as described (Leibfried et al., 2005). Because of the spatial restriction of *WUS* expression, apices of *wus* mutants and moderately expressing *35S::WUS-GR* plants induced with dexamethasone for 4 hr were used as controls and experiment, respectively. Enrichment of an *ARR7* upstream region served as a positive control.

ChIP-chip Sample Preparation

ChIP DNA was blunt-ended and phosphorylated using T4 DNA polymerase and T4 polynucleotide kinase. Linkers were annealed by heating oligos

G-10324 5′-GCGGTGACCCGGGAGATCTGAATTC-3′ and G-10325 5′-GAATTCAGATC-3′ and ligated to ChIP DNA. Two rounds of PCR (22 cycles and 8 cycles) with a dNTP/dUTP mixture and primer G-10324 were conducted before 200 ng DNA were fragmented and labeled with the GeneChip WT double-stranded DNA terminal labeling kit. Samples were hybridized to GeneChip *Arabidopsis* tiling 1.0R arrays. We processed eight samples (four biological replicates in two technical replicates each) of DEX-induced *35S::WUS-GR* and five samples (three biological samples and one biological sample in two technical replicates) of the *wus* mutant.

ChIP-chip Data Analysis

After standard scanning with an Affymetrix 7G Scanner, CEL files were preprocessed with the Affymetrix TAS program using quantile normalization (Kampa et al., 2004). The normalized CEL files were then divided into treatment (*35S::WUS-GR* samples) and control groups (*wus* samples). A two-sample Wilcoxon signed-rank test was conducted on the PM probes with a 250-bp window using Affymetrix TAS. Using the same CEL files divided into treatment and control groups, Tilemap and MAT were run using standard parameters (Ji and Wong, 2005; Johnson et al., 2006). SeedXrich was fed with probe values derived from the Wilcoxon signed-rank test. It systematically combined different parameters to call enriched regions. Those parameters were: (1) number of probes below a defined p value threshold, (2) a local p value minimum (seed), and (3) the number of probes allowed as gaps within called regions. For each combination of parameters, the detected regions were registered. Gene assignment was performed if a region was located within 2000 bp upstream or 300 bp downstream of the transcription start site, in an intron, or 300 bp downstream of the gene model. The parameter space was systematically explored and each combination of settings produced a list of called regions and thus of assigned genes. These lists were solely generated based on the hybridization signals of the ChIP-chip. Subsequently, the proportion of genes with a WRS corresponding to p values below $p < 0.01$ or $p < 0.05$ was recorded for each of those lists. Lists of adequate sizes were randomly sampled for 10,000 times and the same data as for the parameter combinations was recorded. From those distributions, empirical p values for the likelihood of the random occurrence of a proportion of genes with a significant WRS were derived. The results of the parameter combinations and the data of the empirical $p < 0.01$ were plotted (Figures S2B and S2C). An expectation score was calculated by dividing the proportion of called WUS-responsive genes by the proportion at $p < 0.01$. The initial list of the 136 regions used for motif detection was chosen by the convergence of expectation scores for WRS $p < 0.01$ and WRS $p < 0.05$. The settings were: probe p value seed, $p < 0.0004$; probe p value, $p < 0.002$; minimum length of hybridization, 10 probes; maximum gap, three probes.

Use of the same approach generated the final list of 164 enriched regions, but instead of using the WRS as a postdetection benchmark, the occurrence of the TCACGTGA motif in the central 500 bp of the called regions was evaluated. The settings for the optimal detection of WUS binding sites were: probe p value seed, $p < 0.00006$; probe p value, $p < 0.002$; minimum length of hybridization, six probes; maximum gap, one probe. The source code of the program is available on request.

Motif Detection

MDSCAN (Liu et al., 2002) and TRAWLER (Ettwiller et al., 2007) were used for motif detection. For MDSCAN, the 500 nucleotides surrounding the seed of enriched regions were used, and genes with significant WRS ($p < 0.05$) were prioritized. For TRAWLER, full-length enriched sequences and 4800 randomly selected upstream regions were used.

GO Enrichment Analysis

GO enrichment analysis was conducted by using the BINGO 2.3 plug-in (Maere et al., 2005) in Cytoscape 2.6.1 (Shannon et al., 2003) with GO-Terms retrieved from NCBI on August 5th 2008. To test for enrichment, a hypergeometric test was conducted and the Benjamini & Hochberg false discovery rate was calculated. The network of the enriched categories was exported and processed further in yED (http://www.yworks.com/en/products_yed_about.html) with the "organic layout" option.

Computer Simulation of Regulatory Interactions

Using SIMPLEX (Vercruysse and Kuiper, 2005), the WUS/CLV3 system was initially modeled using the following parameters: if true, then WUS 10; if WUS > 10, then CLV3 5; if CLV3 > 10, then WUS −2; if CLV3 > 15, then WUS −8.

The WUS/CLV1/CLV3 system was initially modeled using the following parameters: if true, then WUS 10; if true, then CLV1 10; if WUS > 10, then CLV3 5; if WUS > 3, then CLV1 −9; if CLV1 > 10 and CLV3 > 5, then WUS −2; if CLV1 > 5 and CLV3 > 10, then WUS −2; if CLV1 > 10 and CLV3 > 10, then WUS −8.

For exploring different levels of static induction of *WUS* expression, the *WUS* synthesis value per round of 10 was substituted as depicted in Figure S5B.

In Situ Hybridization

In situ hybridization was performed in accordance with standard protocols (Weigel and Glazebrook, 2002) with the addition of 10% poly(vinyl alcohol) (molecular mass, 70–100 kDa) to the staining solution.

Cloning, Expression, and Purification of Recombinant Proteins

The WUS homeodomain (WUSHD) coding sequence (amino acids 2–168) was amplified using oligos WUS1: 5′-GGGGGATCCAGCCGCCACAGCATCAGC-3′ and WUS2: 5′-GGGGAATTCACTCATGTAGCCATTAGAAGC-3′ and inserted into pGEX-3X (Smith and Johnson, 1988). Full-length *WUS* was cloned into pGEX-6P-1 (GE Healthcare). For expression, *E. coli* cells [strains BL21(DE3) and JM109] were used as described (Palena et al., 1998). Recombinant proteins were purified as described (Smith and Johnson, 1988). The preparation of yeast extracts has been described in Lohmann et al. (2001).

DNA Binding Assays

Aliquots of purified proteins were incubated with double-stranded DNA (0.3–0.6 ng, 30,000 c.p.m., labeled by filling-in the 3′ ends using Klenow fragment) generated by annealing oligos 5′-gATCCTTAcatcgtcGtcAgCTgAtgggATATgCg-3′ and 5′-AATTCgCATATcccaTcAgCTgaCgacgatgTAAg-3′ or derivatives with modifications within the binding sequence. Binding reactions (20 μl) containing 20 mM HEPES (pH 7.5), 50 mM KCl, 2 mM $MgCl_2$, 0.5 mM EDTA, 1.0 mM dithiothreitol, 0.5% Triton X-100, 22 ng/μl BSA, 1 μg poly(-dI-dC), and 10% glycerol were incubated for 15 min at room temperature, supplemented with 2.5% Ficoll, and immediately loaded onto a running gel (5% acrylamide, 0.08% bis-acrylamide in 0.5 × TGE plus 2.5% glycerol [1 × TGE = 25 mM Tris], 190 mM glycine [pH 8.3], 1 mM EDTA). The gel was run in 1 × TGE at 30 mA for 1.5 hr and dried prior to autoradiography. For competition assays, 100-fold excess of unlabeled double-stranded oligos was preincubated for 10 min before the addition of the labeled probe. EMSAs with yeast extracts were performed as described (Lohmann et al., 2001).

Binding Site Selection (SELEX)

For SELEX (Oliphant et al., 1989) procedures described in Blackwell and Weintraub (1990) were used. A labeled 51-mer double-stranded oligo containing a 12-bp random central core (5′-GATGAAGCTTCCTGGACAAT(**12N**)GCAGTCACTGAAGAATTCT-3′) was incubated with purified GST-WUSHD. Bound DNA molecules were isolated via EMSA and eluted from gel slices with 0.5 ml of 0.5 M NH_4Ac, 10 mM $MgCl_2$, 1 mM EDTA, and 0.1% SDS. DNA was amplified using oligos R1 (5′-GATGAAGCTTCCTGGACAAT-3′) and R2 (5′-CAGAATTCTTCAGTGACTGC-3′). After seven selection rounds, the oligonucleotide population was cloned, and random clones were sequenced.

Determination of Dissociation Constant for Full-Length WUS-DNA Interaction

The dissociation constant of WUS as a dimer with DNA was calculated as described (Palena et al., 1999).

Protein-Protein Interaction Test

The WUS C terminus (WUS-C) from nucleotides 349–879 was cloned into *pGADT7* (*pSH074*) and *pGBKT7* (*pSH076*), and interaction was tested following instructions (Clontech).

Reporter Gene Assays in Plant Cells

Agrobacterium tumefaciens harboring the reporter or overexpression constructs were grown at 28°C for 2 days. Cells were harvested and resuspended in 10 mM MES, 10 mM $MgCl_2$, and 150 μM acetosyringone and infiltrated into the abaxial leaf surface of 3-week-old *N. benthamiana* plants after 2 hr. The silencing supressor *35S::P19* was coinfiltrated. After 4 days, leaves were harvested and quantitative real-time RT-PCR was performed as described (Andersen et al., 2008). Tobacco *ACTIN* (accession number: U60495) (5′-CCGGCTATGTATGTTGCTAT-3′ and 5′-TCGTAGATAGGGACAG TGTGA-3′) and the kanamycin resistance gene (5′-CGTCTTGGAGTTCATTC AGG-3′ and 5′-TGGAGAGGCTATTCGGCTAT-3′) served as a reference.

ACCESSION NUMBERS

Microarray data are available under ArrayExpress accession number E-MEXP-2499.

SUPPLEMENTAL INFORMATION

Supplemental Information includes five figures, five tables, and Supplemental Experimental Procedures and can be found with this article online at doi:10.1016/j.devcel.2010.03.012.

ACKNOWLEDGMENTS

We thank Thomas Laux for sharing the WUS cDNA, Annette Maier for sharing material, Detlef Weigel and the Lohmann Lab for discussion, and Philip Benfey, Thomas Holstein, Kay Schneitz, and Detlef Weigel for critical reading of the manuscript. This work was supported by a Career Development Award of the International Human Frontier Science Program Organization, an EMBO Young Investigator Award, ERA-PG grant "Ciscode" DFG LO1450/1-1, and the CellNetworks–Cluster of Excellence (to J.U.L.); a Ph.D. fellowship of the Cusanuswerk (to W.B.); CONICET, FONCyT, and UNL grants (to R.C.); and the Max Planck Society.

W.B., A.L., and J.U.L. performed the transcriptome analyses; W.B. performed ChIP-chip experiments; A.M., F.D.A., and R.L.C. performed in vitro binding assays and SELEX; J.F., G.D., and T.S. performed reporter gene assays; W.B. and C.S. performed qRT-PCRs; S.H. and A.M. performed protein interaction tests; W.B. and Z.Z. performed in situ hybridizations; W.B., S.J.S., and N.H. performed bioinformatic analyses; and W.B. and J.U.L. wrote the paper.

Received: July 29, 2009
Revised: February 3, 2010
Accepted: March 2, 2010
Published: May 17, 2010

REFERENCES

Agashe, B., Prasad, C.K., and Siddiqi, I. (2002). Identification and analysis of DYAD: a gene required for meiotic chromosome organisation and female meiotic progression in Arabidopsis. Development *129*, 3935–3943.

Alon, U. (2007). Network motifs: theory and experimental approaches. Nat. Rev. Genet. *8*, 450–461.

Andersen, S.U., Buechel, S., Zhao, Z., Ljung, K., Novak, O., Busch, W., Schuster, C., and Lohmann, J.U. (2008). Requirement of B2-type cyclin-dependent kinases for meristem integrity in Arabidopsis thaliana. Plant Cell *20*, 88–100.

Berger, M.F., Badis, G., Gehrke, A.R., Talukder, S., Philippakis, A.A., Pena-Castillo, L., Alleyne, T.M., Mnaimneh, S., Botvinnik, O.B., Chan, E.T., et al. (2008). Variation in homeodomain DNA binding revealed by high-resolution analysis of sequence preferences. Cell *133*, 1266–1276.

Blackwell, T.K., and Weintraub, H. (1990). Differences and similarities in DNA-binding preferences of MyoD and E2A protein complexes revealed by binding site selection. Science *250*, 1104–1110.

Blackwell, T.K., Kretzner, L., Blackwood, E.M., Eisenman, R.N., and Weintraub, H. (1990). Sequence-specific DNA binding by the c-Myc protein. Science *250*, 1149–1151.

Bowman, J.L., Smyth, D.R., and Meyerowitz, E.M. (1989). Genes directing flower development in *Arabidopsis*. Plant Cell *1*, 37–52.

Bowman, J.L., Alvarez, J., Weigel, D., Meyerowitz, E.M., and Smyth, D.R. (1993). Control of flower development in *Arabidopsis thaliana* by *APETALA1* and interacting genes. Development *119*, 721–743.

Brand, U., Fletcher, J.C., Hobe, M., Meyerowitz, E.M., and Simon, R. (2000). Dependence of stem cell fate in *Arabidopsis* on a feedback loop regulated by *CLV3* activity. Science *289*, 617–619.

Brand, U., Grunewald, M., Hobe, M., and Simon, R. (2002). Regulation of CLV3 expression by two homeobox genes in Arabidopsis. Plant Physiol. *129*, 565–575.

Chilley, P.M., Casson, S.A., Tarkowski, P., Hawkins, N., Wang, K.L., Hussey, P.J., Beale, M., Ecker, J.R., Sandberg, G.K., and Lindsey, K. (2006). The POLARIS peptide of Arabidopsis regulates auxin transport and root growth via effects on ethylene signaling. Plant Cell *18*, 3058–3072.

Chini, A., Fonseca, S., Fernandez, G., Adie, B., Chico, J.M., Lorenzo, O., Garcia-Casado, G., Lopez-Vidriero, I., Lozano, F.M., Ponce, M.R., et al. (2007). The JAZ family of repressors is the missing link in jasmonate signalling. Nature *448*, 666–671.

Clark, S.E., Running, M.P., and Meyerowitz, E.M. (1993). CLAVATA1, a regulator of meristem and flower development in Arabidopsis. Development *119*, 397–418.

Clark, S.E., Running, M.P., and Meyerowitz, E.M. (1995). *CLAVATA3* is a specific regulator of shoot and floral meristem development affecting the same processes a *CLAVATA1*. Development *121*, 2057–2067.

Clark, S.E., Williams, R.W., and Meyerowitz, E.M. (1997). The *CLAVATA1* gene encodes a putative receptor kinase that controls shoot and floral meristem size in Arabidopsis. Cell *89*, 575–585.

Deyhle, F., Sarkar, A.K., Tucker, E.J., and Laux, T. (2007). WUSCHEL regulates cell differentiation during anther development. Dev. Biol. *302*, 154–159.

Ding, Y.H., Liu, N.Y., Tang, Z.S., Liu, J., and Yang, W.C. (2006). Arabidopsis GLUTAMINE-RICH PROTEIN23 is essential for early embryogenesis and encodes a novel nuclear PPR motif protein that interacts with RNA polymerase II subunit III. Plant Cell *18*, 815–830.

Eilers, M., and Eisenman, R.N. (2008). Myc's broad reach. Genes Dev. *22*, 2755–2766.

Ettwiller, L., Paten, B., Ramialison, M., Birney, E., and Wittbrodt, J. (2007). Trawler: de novo regulatory motif discovery pipeline for chromatin immunoprecipitation. Nat. Methods *4*, 563–565.

Farnham, P.J. (2009). Insights from genomic profiling of transcription factors. Nat. Rev. Genet. *10*, 605–616.

Feng, H., Chen, Q., Feng, J., Zhang, J., Yang, X., and Zuo, J. (2007). Functional characterization of the Arabidopsis eukaryotic translation initiation factor 5A-2 that plays a crucial role in plant growth and development by regulating cell division, cell growth, and cell death. Plant Physiol. *144*, 1531–1545.

Fletcher, J.C., Brand, U., Running, M.P., Simon, R., and Meyerowitz, E.M. (1999). Signaling of cell fate decisions by *CLAVATA3* in *Arabidopsis* shoot meristems. Science *283*, 1911–1914.

Fulton, L., Batoux, M., Vaddepalli, P., Yadav, R.K., Busch, W., Andersen, S.U., Jeong, S., Lohmann, J.U., and Schneitz, K. (2009). DETORQUEO, QUIRKY, and ZERZAUST represent novel components involved in organ development mediated by the receptor-like kinase STRUBBELIG in Arabidopsis thaliana. PLoS Genet. *5*, e1000355.

Gentleman, R.C., Carey, V.J., Bates, D.M., Bolstad, B., Dettling, M., Dudoit, S., Ellis, B., Gautier, L., Ge, Y., Gentry, J., et al. (2004). Bioconductor: open software development for computational biology and bioinformatics. Genome Biol. *5*, R80.

Grooteclaes, M.L., and Frisch, S.M. (2000). Evidence for a function of CtBP in epithelial gene regulation and anoikis. Oncogene *19*, 3823–3828.

Gross-Hardt, R., Lenhard, M., and Laux, T. (2002). WUSCHEL signaling functions in interregional communication during Arabidopsis ovule development. Genes Dev. *16*, 1129–1138.

Hueber, S.D., Bezdan, D., Henz, S.R., Blank, M., Wu, H., and Lohmann, I. (2007). Comparative analysis of Hox downstream genes in Drosophila. Development *134*, 381–392.

Ikeda, M., Mitsuda, N., and Ohme-Takagi, M. (2009). Arabidopsis WUSCHEL is a bifunctional transcription factor that acts as a repressor in stem cell regulation and as an activator in floral patterning. Plant Cell *21*, 3493–3505.

Jaillais, Y., Fobis-Loisy, I., Miege, C., Rollin, C., and Gaude, T. (2006). AtSNX1 defines an endosome for auxin-carrier trafficking in Arabidopsis. Nature *443*, 106–109.

Ji, H., and Wong, W.H. (2005). TileMap: create chromosomal map of tiling array hybridizations. Bioinformatics *21*, 3629–3636.

Johnson, W.E., Li, W., Meyer, C.A., Gottardo, R., Carroll, J.S., Brown, M., and Liu, X.S. (2006). Model-based analysis of tiling-arrays for ChIP-chip. Proc. Natl. Acad. Sci. USA *103*, 12457–12462.

Kampa, D., Cheng, J., Kapranov, P., Yamanaka, M., Brubaker, S., Cawley, S., Drenkow, J., Piccolboni, A., Bekiranov, S., Helt, G., et al. (2004). Novel RNAs identified from an in-depth analysis of the transcriptome of human chromosomes 21 and 22. Genome Res. *14*, 331–342.

Kieffer, M., Stern, Y., Cook, H., Clerici, E., Maulbetsch, C., Laux, T., and Davies, B. (2006). Analysis of the transcription factor WUSCHEL and its functional homologue in Antirrhinum reveals a potential mechanism for their roles in meristem maintenance. Plant Cell *18*, 560–573.

Kojima, H., Suzuki, T., Kato, T., Enomoto, K., Sato, S., Kato, T., Tabata, S., Saez-Vasquez, J., Echeverria, M., Nakagawa, T., et al. (2007). Sugar-inducible expression of the nucleolin-1 gene of Arabidopsis thaliana and its role in ribosome synthesis, growth and development. Plant J. *49*, 1053–1063.

Kondo, T., Sawa, S., Kinoshita, A., Mizuno, S., Kakimoto, T., Fukuda, H., and Sakagami, Y. (2006). A plant peptide encoded by CLV3 identified by in situ MALDI-TOF MS analysis. Science *313*, 845–848.

Laux, T., Mayer, K.F., Berger, J., and Jürgens, G. (1996). The WUSCHEL gene is required for shoot and floral meristem integrity in Arabidopsis. Development *122*, 87–96.

Leatherman, J.L., and Dinardo, S. (2008). Zfh-1 controls somatic stem cell self-renewal in the Drosophila testis and nonautonomously influences germline stem cell self-renewal. Cell Stem Cell *3*, 44–54.

Leibfried, A., To, J.P., Busch, W., Stehling, S., Kehle, A., Demar, M., Kieber, J.J., and Lohmann, J.U. (2005). WUSCHEL controls meristem function by direct regulation of cytokinin-inducible response regulators. Nature *438*, 1172–1175.

Lenhard, M., Jurgens, G., and Laux, T. (2002). The WUSCHEL and SHOOTMERISTEMLESS genes fulfil complementary roles in Arabidopsis shoot meristem regulation. Development *129*, 3195–3206.

Li, J., Yang, H., Peer, W.A., Richter, G., Blakeslee, J., Bandyopadhyay, A., Titapiwantakun, B., Undurraga, S., Khodakovskaya, M., Richards, E.L., et al. (2005). Arabidopsis H+-PPase AVP1 regulates auxin-mediated organ development. Science *310*, 121–125.

Liu, X.S., Brutlag, D.L., and Liu, J.S. (2002). An algorithm for finding protein-DNA binding sites with applications to chromatin-immunoprecipitation microarray experiments. Nat. Biotechnol. *20*, 835–839.

Lohmann, J.U., Hong, R.L., Hobe, M., Busch, M.A., Parcy, F., Simon, R., and Weigel, D. (2001). A molecular link between stem cell regulation and floral patterning in Arabidopsis. Cell *105*, 793–803.

Long, J.A., Ohno, C., Smith, Z.R., and Meyerowitz, E.M. (2006). TOPLESS regulates apical embryonic fate in Arabidopsis. Science *312*, 1520–1523.

Maere, S., Heymans, K., and Kuiper, M. (2005). BiNGO: a Cytoscape plugin to assess overrepresentation of gene ontology categories in biological networks. Bioinformatics *21*, 3448–3449.

Maier, A.T., Stehling-Sun, S., Wollmann, H., Demar, M., Hong, R.L., Haubeiss, S., Weigel, D., and Lohmann, J.U. (2009). Dual roles of the bZIP transcription factor PERIANTHIA in the control of floral architecture and homeotic gene expression. Development *136*, 1613–1620.

Mayer, K.F., Schoof, H., Haecker, A., Lenhard, M., Jürgens, G., and Laux, T. (1998). Role of WUSCHEL in regulating stem cell fate in the Arabidopsis shoot meristem. Cell *95*, 805–815.

Menkens, A.E., Schindler, U., and Cashmore, A.R. (1995). The G-box: a ubiquitous regulatory DNA element in plants bound by the GBF family of bZIP proteins. Trends Biochem. Sci. *20*, 506–510.

Nagasaki, H., Matsuoka, M., and Sato, Y. (2005). Members of TALE and WUS subfamilies of homeodomain proteins with potentially important functions in development form dimers within each subfamily in rice. Genes Genet. Syst. *80*, 261–267.

Noyes, M.B., Christensen, R.G., Wakabayashi, A., Stormo, G.D., Brodsky, M.H., and Wolfe, S.A. (2008). Analysis of homeodomain specificities allows the family-wide prediction of preferred recognition sites. Cell *133*, 1277–1289.

Ogawa, M., Shinohara, H., Sakagami, Y., and Matsubayashi, Y. (2008). Arabidopsis CLV3 peptide directly binds CLV1 ectodomain. Science *319*, 294.

Ohyama, K., Shinohara, H., Ogawa-Ohnishi, M., and Matsubayashi, Y. (2009). A glycopeptide regulating stem cell fate in Arabidopsis thaliana. Nat. Chem. Biol. *5*, 578–580.

Oliphant, A.R., Brandl, C.J., and Struhl, K. (1989). Defining the sequence specificity of DNA-binding proteins by selecting binding sites from random-sequence oligonucleotides: analysis of yeast GCN4 protein. Mol. Cell. Biol. *9*, 2944–2949.

Palena, C.M., Gonzalez, D.H., and Chan, R.L. (1999). A monomer-dimer equilibrium modulates the interaction of the sunflower homeodomain leucine-zipper protein Hahb-4 with DNA. Biochem. J. *341*, 81–87.

Palena, C.M., Gonzalez, D.H., Guelman, S.A., and Chan, R.L. (1998). Expression of sunflower homeodomain containing proteins in Escherichia coli: purification and functional studies. Protein Expr. Purif. *13*, 97–103.

Petricka, J.J., and Nelson, T.M. (2007). Arabidopsis nucleolin affects plant development and patterning. Plant Physiol. *144*, 173–186.

Reinhardt, D., Frenz, M., Mandel, T., and Kuhlemeier, C. (2003). Microsurgical and laser ablation analysis of interactions between the zones and layers of the tomato shoot apical meristem. Development *130*, 4073–4083.

Scheres, B. (2007). Stem-cell niches: nursery rhymes across kingdoms. Nat. Rev. Mol. Cell Biol. *8*, 345–354.

Schmid, M., Davison, T.S., Henz, S.R., Pape, U.J., Demar, M., Vingron, M., Schölkopf, B., Weigel, D., and Lohmann, J.U. (2005). A gene expression map of Arabidopsis thaliana development. Nat. Genet. *37*, 501–506.

Schoof, H., Lenhard, M., Haecker, A., Mayer, K.F., Jurgens, G., and Laux, T. (2000). The stem cell population of Arabidopsis shoot meristems in maintained by a regulatory loop between the CLAVATA and WUSCHEL genes. Cell *100*, 635–644.

Shannon, P., Markiel, A., Ozier, O., Baliga, N.S., Wang, J.T., Ramage, D., Amin, N., Schwikowski, B., and Ideker, T. (2003). Cytoscape: a software environment for integrated models of biomolecular interaction networks. Genome Res. *13*, 2498–2504.

Siddiqi, I., Ganesh, G., Grossniklaus, U., and Subbiah, V. (2000). The dyad gene is required for progression through female meiosis in Arabidopsis. Development *127*, 197–207.

Singh, S.K., Eland, C., Harholt, J., Scheller, H.V., and Marchant, A. (2005). Cell adhesion in Arabidopsis thaliana is mediated by ECTOPICALLY PARTING CELLS 1—a glycosyltransferase (GT64) related to the animal exostosins. Plant J. *43*, 384–397.

Smith, D.B., and Johnson, K.S. (1988). Single-step purification of polypeptides expressed in *Escherichia coli* as fusions with glutathione *S*-transferase. Gene *67*, 31–40.

Szemenyei, H., Hannon, M., and Long, J.A. (2008). TOPLESS mediates auxin-dependent transcriptional repression during Arabidopsis embryogenesis. Science *319*, 1384–1386.

Takahashi, K., and Yamanaka, S. (2006). Induction of pluripotent stem cells from mouse embryonic and adult fibroblast cultures by defined factors. Cell *126*, 663–676.

Tanaka, H., Ishikawa, M., Kitamura, S., Takahashi, Y., Soyano, T., Machida, C., and Machida, Y. (2004). The AtNACK1/HINKEL and

STUD/TETRASPORE/AtNACK2 genes, which encode functionally redundant kinesins, are essential for cytokinesis in Arabidopsis. Genes Cells *9*, 1199–1211.

Thines, B., Katsir, L., Melotto, M., Niu, Y., Mandaokar, A., Liu, G., Nomura, K., He, S.Y., Howe, G.A., and Browse, J. (2007). JAZ repressor proteins are targets of the SCF(COI1) complex during jasmonate signalling. Nature *448*, 661–665.

To, J.P., Haberer, G., Ferreira, F.J., Deruere, J., Mason, M.G., Schaller, G.E., Alonso, J.M., Ecker, J.R., and Kieber, J.J. (2004). Type-A Arabidopsis response regulators are partially redundant negative regulators of cytokinin signaling. Plant Cell *16*, 658–671.

Trotochaud, A.E., Hao, T., Wu, G., Yang, Z., and Clark, S.E. (1999). The CLAVATA1 receptor-like kinase requires CLAVATA3 for its assembly into a signaling complex that includes KAPP and a Rho-related protein. Plant Cell *11*, 393–406.

Vercruysse, S., and Kuiper, M. (2005). Simulating genetic networks made easy: network construction with simple building blocks. Bioinformatics *21*, 269–271.

Weigel, D., and Glazebrook, J. (2002). Arabidopsis: A Laboratory Manual (Cold Spring Harbor, NY: Cold Spring Harbor Laboratory Press).

Weigel, D., and Jürgens, G. (2002). Stem cells that make stems. Nature *415*, 751–754.

Wu, Z., Irizarry, R.A., Gentleman, R., Murillo, F.M., and Spencer, F.A. (2004). A model based background adjustment for oligonucleotide expression arrays. Working Paper 1. Department of Biostatistics Working Papers (Baltimore, MD: The Johns Hopkins University).

Yadav, R.K., Girke, T., Pasala, S., Xie, M., and Reddy, G.V. (2009). Gene expression map of the Arabidopsis shoot apical meristem stem cell niche. Proc. Natl. Acad. Sci. USA *106*, 4941–4946.

Zeller, G., Clark, R.M., Schneeberger, K., Bohlen, A., Weigel, D., and Ratsch, G. (2008). Detecting polymorphic regions in Arabidopsis thaliana with resequencing microarrays. Genome Res. *18*, 918–929.